

Optimal Layering Time Control for Stepped-Concurrent Radiative Curing Process

Adamu Yebi¹

Automotive Engineering Department,
Clemson University—International Center for
Automotive Research,
Greenville, SC 29607
e-mail: ayebi@clemson.edu

Beshah Ayalew

Mem. ASME
Automotive Engineering Department,
Clemson University—International Center for
Automotive Research,
Greenville, SC 29607
e-mail: beshah@clemson.edu

This paper makes the following main proposals: (1) a stepped-concurrent curing (SCC) approach for making thick parts using ultraviolet (UV) radiative curing and (2) an optimal interlayer hold time control scheme to maximize the benefit of the SCC approach. The SCC approach seeks to reduce cure level deviations across a thick part by introducing new layers before earlier ones cure completely. A model of the UV curing process that includes the coupled cure kinetics and heat transfer is used to motivate the SCC scheme as well as the inherent optimization problem in this process. Then, the SCC process is cast as a hybrid system in which the addition of each layer switches the underlying state space to one with a higher dimension. Minimization of the overall cure deviation is set as the objective of the process and the necessary conditions for the optimal interlayer hold time control sequence are explicitly derived and solved via a steepest descent algorithm. Applications of the proposed scheme to a composite laminate curing process show that the so computed optimal layering time control sequence indeed gives the best performance in terms of closely tracking a target cure level distribution, compared to equal-time SCC or one-shot curing of the whole thick part. [DOI: 10.1115/1.4029023]

Keywords: UV curing, additive manufacturing, optimal layering control, composite processing

1 Introduction

Over the last two decades, the range of applications for UV radiation curing of materials has been growing steadily. The common ones include photopolymerization of thin film/section paints and coatings, color proofing, letter pressing, microelectronics production, and dental fillings. It is also been used in layer-by-layer manufacturing of thicker parts via stereolithography (STL) and related rapid prototyping and manufacturing processes [1]. UV curing is also gaining a substantial interest for curing composite laminates due to its advantages of accelerated processing time, higher-energy efficiency, less environmental pollution, reduced space usage, and better controllability [2,3].

Despite these stated advantages, the thickness of parts that can be cured effectively by direct UV radiation is limited because of the attenuation of UV as it passes through the target materials [4]. As a result, extended irradiation may be needed to cure thick sections. However, in thick sections, the accompanying thermal and cure level gradients from the exothermic cure reactions may compromise the quality and mechanical performance of the end product. This is often overcome by offline optimization of process parameters such as the concentration of photoinitiators, the position of UV source, and intensity settings. Such optimization only yields good results for parts of limited thickness (<4 mm) [5]. To overcome this fundamental limitation, an approach of layer-by-layer deposition and curing has been in use for additive manufacturing of thicker sections [6] and has also recently been proposed for curing of composite laminates [7].

There are some persistent challenges that still need to be addressed in layer-by-layer UV curing for additive manufacturing of thicker sections. One of the challenges is differing material shrinkage between layers, which in STL processes causes

dimensional inaccuracy and the well-known staircase effect [6]. The differing material shrinkage is more pronounced when the multilayer part experiences high cure level gradients across its depth [8]. A related challenge is the development of excessive thermal stresses in layers exposed to UV radiation for prolonged time. In the current practice of layer-by-layer curing, a new layer is added after the previous layer is cured completely or is near to complete cure. As a result, the extra UV radiation exposure reaching the already cured layers and associated heating may result in breakage of molecular bonds [9]. The combination of material shrinkage and continuous heating of cured layers may cause a complex stress state responsible for overall distortions in the end product. This is also true for parts produced via additive manufacturing involving metal powder deposition [10].

Some practical solutions have been proposed to overcome these challenges. In Ref. [6], a stepless rapid prototyping system was proposed that combines layer-by-layer manufacturing with intermediate use of five-axis Computer Numerical Control (CNC) technology to improve the dimensional accuracy. In Ref. [11], for selective laser sintering application, Wang developed a shrinkage model to determine a scaling factor that can be input to CAD models for the compensation of shrinkage. In another study [12], the need for modifying STL file algorithm is highlighted to reduce geometric error while converting CAD models to STL files. These developments may improve the dimensional accuracy of the end product, but they do not directly influence the inherent processes (cure level and thermal gradients) that lead to the distortions in the first place. On the other hand, there is at least one experimental evidence [7] which showed that the mechanical properties of a fiber glass composite product improves significantly by partially curing the bottom layers before adding the top layers. However, the full optimizability of this approach has not been investigated.

In this paper, we propose a stepped-concurrent layering and (SCC) approach for thick part manufacturing and outline optimal layering considerations for its successful implementation. SCC is a variation of a layer-by-layer curing where the new layers are added before previous ones cure completely as suggested in

¹Corresponding author.

Contributed by the Manufacturing Engineering Division of ASME for publication in the JOURNAL OF MANUFACTURING SCIENCE AND ENGINEERING. Manuscript received July 8, 2014; final manuscript received October 29, 2014; published online December 5, 2014. Assoc. Editor: Donggang Yao.

Ref. [7], but in such a way that there is an effective reduction of cure level deviation across all layers. We use a curing process model describing the cure kinetics, UV attenuation and temperature evolution, to explicitly illustrate the potential of the SCC approach via different choices for interlayer hold times for a given UV intensity setting. We then develop a systematic model-based dynamic optimization scheme that fully exploits this potential.

The basic intuition of formulating the SCC process as an optimization problem is drawn from studying the nature of the process. The spatial domains and the initial conditions for the physical processes change with each layer addition, and this influences the achievable cure level deviation across all layers. This intuition also suggests that the SCC process is a hybrid dynamical system in which the addition of each layer represents a discrete event on the underlying continuous curing and thermal dynamics. Using finite dimensional representations for the underlying dynamics in each layer, we observe that the SCC represents a multimode hybrid system with a predefined mode sequence of increasing state dimensions. We treat the times between layer additions (interlayer hold times) as the control variables. We then derive the necessary conditions for optimality by customizing the theory developed for general hybrid systems [13,14] to this application in additive manufacturing. A computational algorithm is provided that can be used to solve for optimal interlayer hold times that give minimal cure level deviations in the SCC approach. We illustrate the effectiveness of the algorithm by applying the SCC approach to simulations of a fiberglass composite part layering and curing process.

It seems there are few other works that take the formal dynamic optimization approach for such processes. The closest one found is the one in Ref. [15] which suggested optimization of the laminator temperature in a thermal curing process for fabricating a composite part by laminated object manufacturing method. However, the work in Ref. [15] dealt with optimizing prescribed laminator temperature profiles (with time) which restricts the solution. We remark that the treatment of the layer-by-layer curing process as a hybrid system is likely a first contribution of the present paper.

The remainder of the paper is organized as follows. Section 2 gives further background and modeling considerations for the UV curing process and details a generalized 1D model for the process. Section 3 motivates the SCC approach. Section 4 details the formulation of the SCC process as hybrid system, derives the optimality conditions, and lists an algorithm for the optimal interlayer hold times. Section 5 includes demonstrative numerical simulation results and discussions. Section 6 gives the conclusions of the work. An appendix and a nomenclature list are provided at the end.

2 Modeling the UV Curing Process

2.1 Background and Modeling Considerations.

UV curing allows fast transformation of a liquid resin into a cross-linked solid structure by photopolymerization of a resin formulation containing UV sensitive photoinitiators and monomers [16]. When the target resin is irradiated with UV, the photoinitiator molecules absorb photons and form excited radicals that facilitate the photopolymerization reactions. The rate of this reaction is affected by the local intensity and the duration of exposure of the target resin material to UV radiation. In addition, the UV curing process involves heat transfer phenomena including heat generated by the exothermic cure reaction, heat conduction in the target, and convective (and some radiative) heat transfer between the surrounding environment and the target. These cure kinetics and the heat transfer are coupled phenomena that can be captured with a well-crafted mathematical model.

There are a few previous works focused on the physical/mathematical modeling of the UV curing process for STL applications [17–19] and at least one for UV composite processing via

filament winding [20]. The physical model for UV curing differs from that of the more common thermal (open air, autoclave, or oven) curing due to two main considerations. The first consideration is that, in UV curing, the cure kinetics model should incorporate the spatial attenuation of UV intensity with depth (resin thickness) due to photo-absorption. This is often called the Beer-Lambert effect [1]. This effect is especially relevant for thick targets. For UV curing, this attenuating input is modeled as an in-domain input, unlike in thermal curing where the convective/radiative input is often modeled as a boundary input. The second consideration is that, for the heat transfer model, in addition to the exothermic cure reactions, a term for heat generation from direct absorption of UV radiation needs to be introduced for UV curing.

When considering the UV curing process for thick sections (>1 mm), the choice of thermal boundary conditions is especially important [21]. This is because of the dominant coupling of the UV polymerization process with thermal effects (for select resin types) [22]. In fact, for a single thick layer or section, by insulating the nonexposed end of the target, it is possible to influence the cure conversion distribution as more energy is retained near the far ends of the thick section in a manner that counteracts the Beer-Lambert effect and helps to reduce cure level deviations across the part [23].

In this paper, we use a UV curing process model that includes the above considerations for thick sections and derive systematic optimality conditions for the SCC approach. Note that, for the SCC process, the layer thickness could be a process design variable that should be predecided for the specific material considering the UV attenuation phenomena.

2.2 Details of Model.

Consider the schematic of the 1D UV curing process for a single resin layer or thick section shown in Fig. 1.

The energy balance during the process is governed by the partial differential equation (PDE) [19,20]

$$c_p \frac{\partial T(z, t)}{\partial t} = \frac{\partial}{\partial z} \left(k_z \frac{\partial T(z, t)}{\partial z} \right) + \dot{q}_{\text{exh}}(z, t) \quad (1)$$

where ρ and c_p are the density and specific heat capacity of the layer, respectively; k_z is the thermal conductivity of the layer across depth; $T(z, t)$ is temperature distribution at depth z and time t . $\dot{q}_{\text{exh}}(z, t)$ is heat generated from exothermic reaction. If this layer is of a composite fiberglass and resin matrix, the average parameters of the resin and fibers can be considered for the matrix [20]. We shall be considering composite applications for the purposes of all simulations presented later.

The cure kinetics model for photopolymerization of an unsaturated polyester resins is given by the nonlinear ordinary differential equation (ODE) [17]

$$\frac{d\alpha(z, t)}{dt} = \phi s^q I^p \exp\left(\frac{-E}{RT_{\text{abs}}(z, t)}\right) \alpha^m(z, t) (1 - \alpha(z, t))^n \quad (2)$$

where E is activation energy, s is photoinitiator concentration, ϕ is pre-exponential rate constant, R is gas constant, I is UV

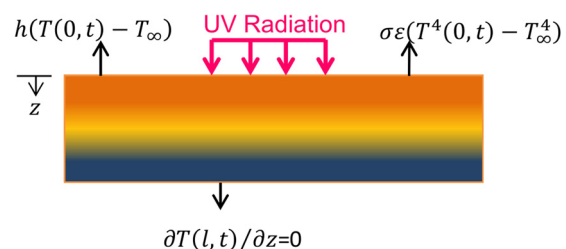


Fig. 1 Schematic of a UV curing process

radiation intensity, T_{abs} is absolute temperature in Kelvin, $\alpha(z, t)$ is cure conversion level distribution, m & n are reaction orders, p & q are constant exponents, and $d\alpha(z, t)/dt$ is the rate of cure conversion (rate of polymerization or rate of cure). The diffusion of specific species (monomers, radicals, and photoinitiators) is assumed to be negligible [24]. The heat released from the exothermic cure reaction is a function of the rate of polymerization (rate of cure)

$$\dot{q}_{\text{exh}}(z, t) = v_r \rho_r \Delta H_r \frac{d\alpha(z, t)}{dt} \quad (3)$$

where ρ_r is density of resin and ΔH_r is polymerization enthalpy of resin. The factor v_r is the volumetric fraction of resin in a composite matrix and is introduced to consider the fact that only the resin portion undergoes the photopolymerization reaction in such a composite ([20,25]). When treating pure resin layers, one may set $v_r = 1$.

The UV intensity I at depth z is attenuated according to Beer-Lambert's law

$$I = I_0 \exp(-\lambda_c z) \quad (4)$$

where I_0 is the incident UV-light intensity at the surface and λ_c is the attenuation constant for the layer. We assume a nonphotobleaching [1] type photoinitiator for this work for which only spatial attenuation is relevant. The analysis can be extended for photobleaching [24] types as well. For a composite layer, the consideration of a single attenuation constant essentially assumes matched refractive indices of the fiber and resin in a uniformly wetted fiberglass and resin [9]. The attenuation constant for the resin alone (λ_r) can be approximated in Ref. [17]

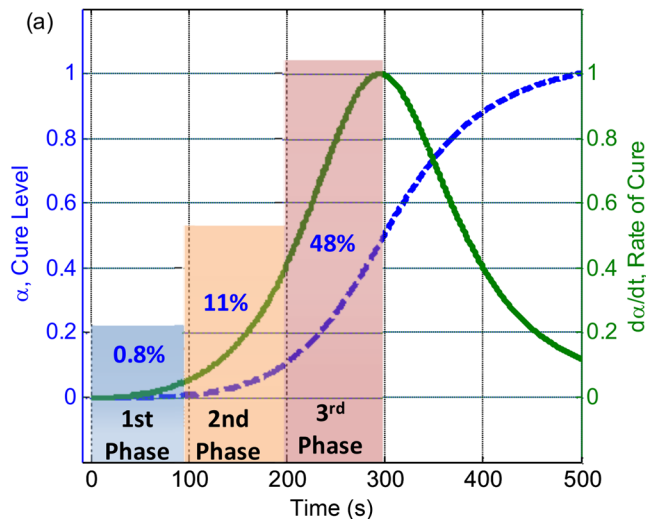
$$\lambda_r = \mu s \quad (5)$$

where μ is the UV absorption coefficient of the photoinitiator and s is the photoinitiator concentration in the resin.

The energy balance equation (1) is not complete without the appropriate boundary conditions for the layer. Just for the schematic of Fig. 1, the following convective and insulated boundary conditions are specified at the top and bottom boundaries:

$$-k_z \frac{\partial T(0, t)}{\partial z} + \vartheta I_0 = h(T(0, t) - T_\infty) \quad (6)$$

$$\frac{\partial T(l, t)}{\partial z} = 0 \quad (7)$$



where h is convective heat transfer at the top boundary; l is the thickness of composite laminate, and T_∞ is constant ambient temperature; ϑ is absorptivity constant of the UV radiation at the surface. Note that, in the layer-by-layer process, these boundary conditions are subject to change as new layers are added. This issue will be discussed further in the Appendix and when we treat the multilayer hybrid process in Sec. 4.

Bringing all of the above together, the complete UV curing process model that considers heat transfer, the attenuation of light intensity, cure kinetics as well as the state boundary conditions is summarized in the following form:

$$\begin{cases} \rho c_p \frac{\partial T(z, t)}{\partial t} = \frac{\partial}{\partial z} \left(k_z \frac{\partial T(z, t)}{\partial z} \right) + v_r \rho_r \Delta H_r \frac{d\alpha(z, t)}{dt} \\ -k_z \frac{\partial T(0, t)}{\partial z} + \vartheta I_0 = h(T(0, t) - T_\infty) \\ \frac{\partial T(l, t)}{\partial z} = 0 \\ \frac{\partial \alpha(z, t)}{\partial t} = \varphi S^q I_0^p \exp(-\lambda_c z) \exp\left(\frac{-E}{RT_{\text{abs}}(z, t)}\right) \alpha^m(z, t) (1 - \alpha(z, t))^n \\ T(z, 0) = T_0(z) \\ \alpha(z, 0) = \alpha_0(z) \end{cases} \quad (8)$$

The last two equations in Eq. (8) are the initial temperature and cure state distributions in the layer. Using this coupled nonlinear PDE-ODE model for the curing process of single layers, we conduct some simulation-based analyses to first motivate the stepped-concurrent layering and curing approach, and subsequently, to systematically optimize it. For the simulation studies, the PDE in Eq. (8) is first transformed to a set of ODEs using a central-in-space finite difference method. Then, the augmented ODE system of both temperature and cure state is solved forward-in-time using Euler's method.

3 Motivation for the SCC Approach

The idea for using SCC to reduce interlayer cure level deviation is arrived at from a close examination of: (i) the evolution of the cure kinetics with time and (ii) the nature of the attenuation of UV radiation with depth. To illustrate these issues, the curing process is simulated with the following conditions: given UV-intensity (65 mW/cm²), photoinitiator concentration (0.05 wt.%), and a single layer of thickness 2 mm. The time evolution of the normalized rate of cure and cure conversion levels for a location at the bottom

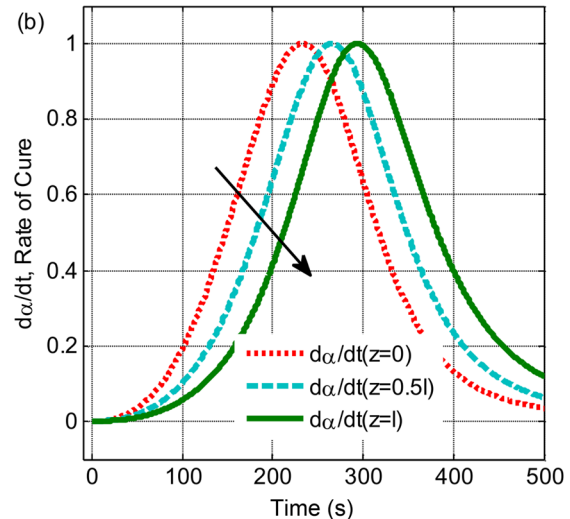


Fig. 2 (a) Propagation of the normalized rate of cure and the cure level at the bottom of the layer ($z = l$); (b) Propagation of the normalized rate of cure in a layer at three different locations. (The normalization is with respect to the maximum value.)

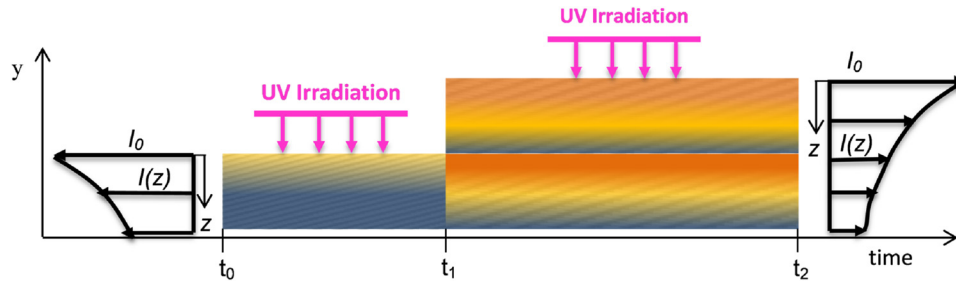


Fig. 3 UV attenuation in a layer-by-layer process (y-axis is used to indicate the direction of part thickness increment as layers add on whereas z-axis indicates the direction of UV attenuation)

of the layer ($z = l$) are plotted in Fig. 2(a). The cure evolution is segmented into three phases. In the first phase, in the first 100 s, only 0.8% of the cure conversion (dotted line) is completed. The rate of cure (solid line) accelerates in the second and third phases with additional conversions of 11% and 48%, respectively, until the rate of cure reaches its peak and begins to slow down.

In Fig. 2(b), the variation of the instantaneous rate of cure across the layer is shown considering top ($z = 0$), middle ($z = 0.5l$), and bottom ($z = l$) locations. The rate of cure decreases in the direction of the arrow from the top to the bottom of the layer as UV radiation gets attenuated with depth. These trends of the cure propagation suggest that there is a decrease in the rate of cure after it peaks, although this happens at different times for different locations in the layer.

We then consider the possibility of curing multiple layers by initiating cure in the earlier (bottom) layer and adding a new layer on top even before the bottom one cures completely. This consideration is further explained with the help of Fig. 3, which shows a two-layer SCC process. Herein, first the UV radiation is applied directly at the top of the bottom layer. This allows the bottom layer to go through its first cure phase quickly. Then, when a second layer is added, the cure propagation continues in the bottom layer with the attenuated UV radiation reaching this layer, while the (new) top layer cures with direct exposure of UV radiation and concurrently goes through its first phase of cure. Therefore, by first initiating the cure in the bottom layer before the second one is added, the instantaneous cure level deviation from the top of the top layer to the bottom of the bottom layer can be kept small thereby reducing cure level gradients and associated thermal

stresses. This approach can also reduce the time required for complete cure of both layers. This SCC of two layers can be readily extended to multiple layers.

In this stepped-concurrent layering and SCC process, given identical photopolymerization parameters (resin composition, UV intensity, location, photoinitiator concentration, etc.) for each layer, there seem to be optimal hold time durations for the inter-layer steps that will give minimal cure level deviation across all layers. This possibility is explored further using a number of simulations of the curing process model given above.

Here, we consider two cases of early and late addition of the new layer for a two-layer part to motivate the need for optimizing the hold time before adding the second layer. The two cases considered for simulation are summarized below.

- Case 1: Early addition: the top layer is added after the bottom layer cured for only 100 s with direct UV exposure.
- Case 2: Late addition: the top layer is added after the bottom layer cured for 300 s with direct UV exposure.

A thickness of 2 mm is considered for each layer. Suppose the desired cure conversion level is 90% with a final cure time of 500 s. We find that, with early addition of the new layer (Fig. 4(a)), the final cure level in the top layer (at $t = 500$ s) already crosses the target value of 90% while the minimum cure level in the bottom layer is near 60%. On the contrary, with late addition of the new layer (Fig. 4(b)), the cure level at the bottom achieves the desired value (with some over cure) while the cure level at the top layer is still at its early phase of cure. Therefore, for this two-layer part, the time hold before the addition of the second layer

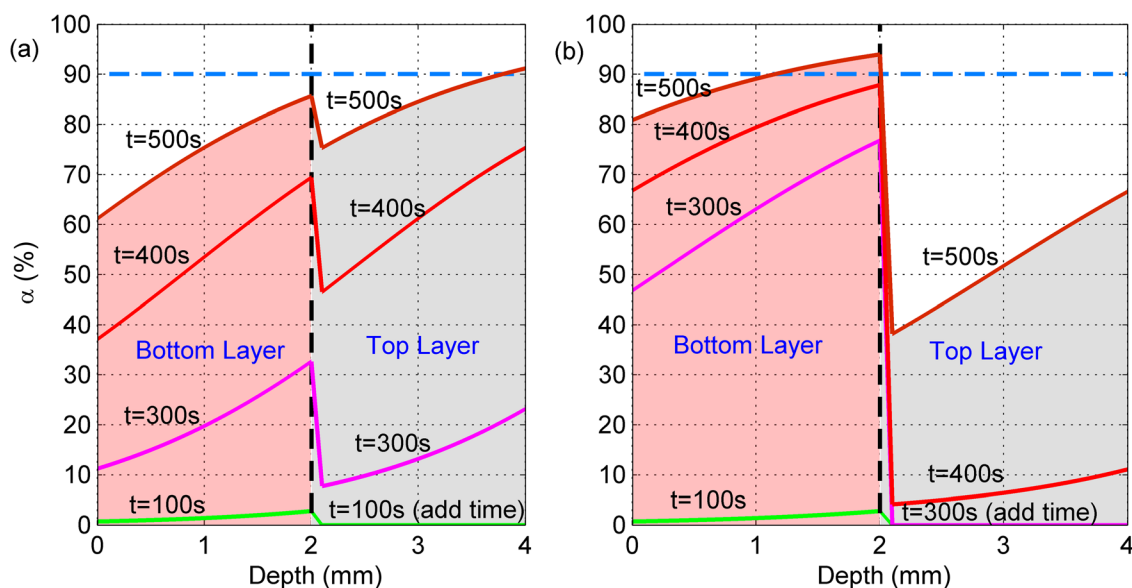


Fig. 4 In process cure level distribution for a two-layer part with (a) early layer addition (at $t = 100$ s) and (b) late layer addition (at $t = 300$ s)

should be selected between these two extremes in order to minimize the cure level deviation.

The determination of the time hold for this two-layer part is an optimization problem that may be solved via a few trials. However, for a general multilayer part, a systematic approach is needed to determine the interlayer time holds (controls). These time-holds should be determined considering the curing process for the complete build of the part. We develop the following model-based optimization scheme to accomplish this.

4 Optimal Layering Time Control

To formulate the SCC approach as a formal optimization problem that can be solved systematically, first we take a closer look at the nature of the process dynamics in SCC. As a new layer is introduced for curing, the spatial domain and boundary conditions for the cure and thermal dynamics switch, resulting in a different process “mode.” This switch of the process mode happens at each layer addition even if the process input UV intensity is kept the same throughout. The switching represents a discrete event, and the switching or layering times are decided externally to the curing process. This is characteristic of a hybrid system where the layering times are control variables that can be manipulated for a desired effect, in our case, for minimization of cure level deviations in a multilayer part.

4.1 Formulation of the SCC Process as a Hybrid System.

To facilitate the discussion and computations, the coupled PDE-ODE system model (8) is first reduced to an augmented nonlinear ODE system by applying central difference approximations for the spatial derivative in the PDE. The resulting system dynamics equations can be written compactly in the form

$$\dot{x}(t) = f(x(t), u(t)), \quad x(0) = x_0 \quad (9)$$

where $x = [T, \alpha]^T$ is the augmented state vector at any time, t , and $u = I_0^p$ is the UV input, x_0 is the initial state vector, and f is a vector function of the spatially discretized state and input. We shall use the same spatial discretization (number of nodes) for each layer and (when necessary) we index the elements of the state vector with spatial location. We use j for indexing the spatial discretization nodes.

The hybrid system view of the SCC approach is depicted schematically in Fig. 5. In the following, a “mode” represents the state dynamics before the addition of a new layer, which serves as the mode switch. The first mode (mode 1) has only one layer, and all other modes have more, in increasing numbers as shown. The

mode switching times are denoted by τ_1 through τ_N . Introducing an identifier i for the mode index, we denote the dimension of the state in mode i by $\dim(x_i) = \bar{n}_i$. Assuming the same size of spatial discretization in each layer, the addition of a second layer in mode 2 increases the dimension of the state by $(\bar{n}_1 - 2)$, where the nodes at the interface of two layers are merged. For any mode i , the state dimension is given by $\bar{n}_i = i(\bar{n}_1 - 2) + 2$. Note also that for the first layer, \bar{n}_1 is equal to twice the number of spatial nodes for the layer, since at each spatial node, we track both temperature and cure state.

This particular hybrid system realization of the SCC process has some specific features: (1) At each mode switch (layer addition), from mode i to the next mode $i + 1$, the dimension of the state vector x increases. (2) Since one can only add layers, the order of the mode switchings is fixed, sequential, and known. (3) All of the mode switching times included in the ordered vector $[\tau_1, \dots, \tau_N]^T$ can be selected independently.

The state evolution for a given mode i in the time interval $[\tau_{i-1}, \tau_i]$ takes the form

$$\dot{x}_i(t) = f_i(x_i(t), u_i(t)), \quad \text{when } t \in [\tau_{i-1}, \tau_i] \quad (10)$$

where $x_i \in \mathcal{R}^{\bar{n}_i}$ is state vector x in mode i , $u_i \in \mathcal{R}^{m_i}$ is continuous time input in mode i , $f_i : \mathcal{R}^{\bar{n}_i} \times \mathcal{R}^{m_i}$ is continuous state transition function in mode i . The form of the function f_i readily follows from the PDE-ODE system (8), with due consideration for the altered boundary conditions following each mode switch. The form of f_i is given in the Appendix.

At each switching time τ_i , the transition to the new mode is described compactly by

$$x_{i+1}(\tau_i^+) = F_i(x_i(\tau_i^-)) \quad (11)$$

where $x_i(\tau_i^-)$ and $x_{i+1}(\tau_i^+)$ are the left hand and right hand limits of the state vector in mode i and mode $i + 1$, respectively, at the switching time τ_i . $F_i : \mathcal{R}^{\bar{n}_i} \rightarrow \mathcal{R}^{\bar{n}_{i+1}}$ is the mode transition operator at switching time τ_i . Note again that the transition is to a higher dimensional mode.

We now discuss the form of the mode transition operator for the SCC process. We enforce continuity in the temperature state at the interface spatial nodes and at new layer addition (switching time) by taking the average temperature of the corresponding nodes as the initial condition for the temperature state corresponding to those nodes in the new mode. The cure state at the interface node is taken as the cure state of the interface node already in the curing process, because cure conversion is an irreversible process.

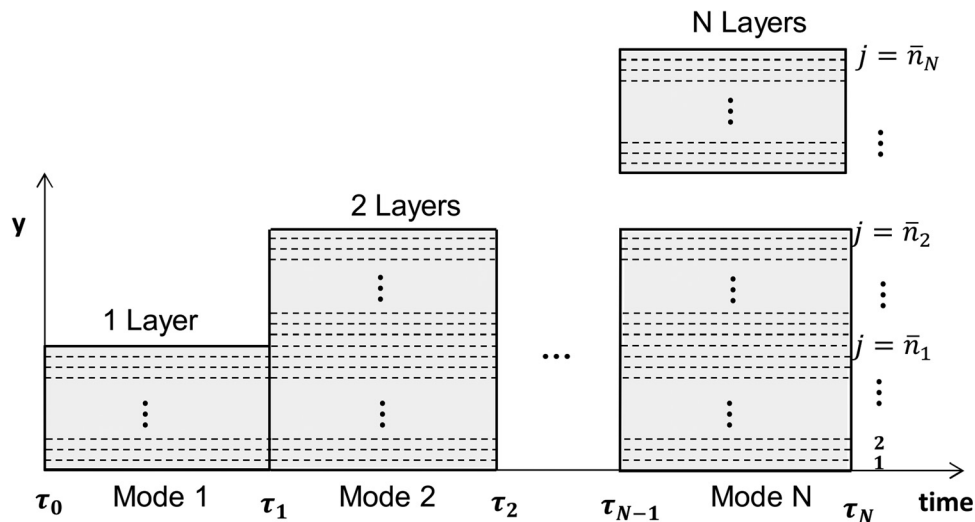


Fig. 5 A hybrid system realization of the SCC process

For all other spatial nodes away from the interface that were already being cured (all previous layers), the initial values of the temperature and cure states in the new mode take their values from the end of previous mode. Of course, the initial value of all state elements corresponding to spatial nodes in the new layer will take on ambient temperature and zero cure values (or some nominal values) in the new mode.

These considerations define the mode transition operator as follows. At this point, we find it necessary to use the spatial node index j in addition to the mode index i to isolate specific state elements.

Temperature state mode transition (superscript T)

$$\begin{aligned} x_{i+1}^T(\tau_i^+) &= F_{i,j}^T(x_{i,j}^T(\tau_i^-)), \quad j = 1, 2, \dots, \bar{n}_{i+1}^T \\ \text{where} \\ F_{i,j}^T(x_{i,j}^T(\tau_i^-)) &= \frac{1}{2} [x_{i,j}^T(\tau_i^-) + T_\infty], \quad j = \bar{n}_i^T \\ F_{i,j}^T(x_{i,j}^T(\tau_i^-)) &= x_{i,j}^T(\tau_i^-), \quad j < \bar{n}_i^T \\ F_{i,j}^T(x_{i,j}^T(\tau_i^-)) &= T_\infty, \quad j > \bar{n}_i^T \end{aligned} \quad (12)$$

Cure state mode transition (superscript α)

$$\begin{aligned} x_{i+1}^\alpha(\tau_i^+) &= F_{i,j}^\alpha(x_{i,j}^\alpha(\tau_i^-)), \quad j = 1, 2, \dots, \bar{n}_{i+1}^\alpha \\ \text{where} \\ F_{i,j}^\alpha(x_{i,j}^\alpha(\tau_i^-)) &= x_{i,j}^\alpha(\tau_i^-), \quad j \leq \bar{n}_i^\alpha \\ F_{i,j}^\alpha(x_{i,j}^\alpha(\tau_i^-)) &= \alpha_0, \quad j > \bar{n}_i^\alpha \end{aligned} \quad (13)$$

where $x_{i,j}^T(\tau_i^-)$ is a left hand limit of the temperature state at switching time τ_i , at a spatial node j in mode i ; \bar{n}_i^T is dimension of the temperature state in mode i . Similar notations are extended to the cure state in Eq. (13). Since we use the same spatial discretization for both, the dimension of the cure state and temperature state are taken here to be the same, $\bar{n}_i^T = \bar{n}_i^\alpha$ and $\bar{n}_i = \bar{n}_i^T + \bar{n}_i^\alpha$. T_∞ denotes ambient temperature.

4.2 Solution of Hybrid System Optimization Problem. For a hybrid system of the form described in Eqs. (10) and (11), the optimal control problem is often posed as one of finding the optimal continuous input $u_i(t)$ and switching time vector $[\tau_1, \dots, \tau_N]^T$ that minimize a cost function that includes running cost and the cost associated with switching the mode of operation. For the proposed SCC process, we are interested in achieving a through cure or near through cure in all layers at the end of the curing process by optimizing only the switching time sequence (layering time) for a given UV radiation input. Hence, the running cost is described by a terminal cost of the form

$$J = \frac{1}{2} \int_{y_0}^{y_N} \{x_N^\alpha(\tau_N) - x_{\text{des}}^\alpha\}^2 dy \quad (14)$$

where $J: \mathcal{R}^{\bar{n}_N/2} \rightarrow \mathcal{R}$ is cost function, x_N^α is the partial state corresponding to the cure level at the last mode of operation, and x_{des}^α is the desired cure level throughout the part at the final time τ_N . y_0 and y_N represent the locations of the bottom end of first layer and the top end of the last layer, respectively. Here, we neglect transition cost for the layering events (assuming each layering event is no different from the others), and we assume instantaneous layering operations.

In the literature, variational calculus is dominantly used to derive the necessary conditions for optimality for hybrid optimization problems, assuming continuity of second derivatives for the functions f_i and J , and, at least of the first derivatives for the function F_i [13,26]. Other proposed solution methods include direct

differentiation of the cost function [27] and two-stage optimization [14]. In this paper, for the hybrid realization of the SCC as described above, we find the variational method readily applicable as outlined in Ref. [28]. The derivation for the necessary conditions for optimality is carried out by adjoining the dynamic constraint (10) and the transition constraint (11) to the cost function (14) using Lagrange multipliers $\bar{p}_i(t) \in \mathcal{R}^{\bar{n}_i}$, $t \in [\tau_{i-1}, \tau_i]$ for Eq. (10) and $\eta_i \in \mathcal{R}^{\bar{n}_{i+1}}$ for Eq. (11), respectively, and defining the Hamiltonian

$$H(x_i, u_i, \bar{p}_i) = \bar{p}' f_i(x_i, u_i) \quad (15)$$

where \bar{p}' is a transpose of \bar{p}_i . The initial time τ_0 and state x_0 are assumed fixed, while the final time τ_N and state $x(\tau_N)$ are free to be optimized.

The optimal control solution for the above hybrid system optimization problem reduces to solving the following equations:

Euler–Lagrange equation

$$\dot{\bar{p}}'_i = - \left(\frac{\partial H_i}{\partial x_i} \right)' \quad (16)$$

Boundary conditions

$$\bar{p}_i(\tau_i^-) = - \left(\frac{\partial F_i}{\partial x_i} \right)' \eta_i \quad (17)$$

$$\eta_i = \bar{p}_{i+1}(\tau_i^+) \quad (18)$$

$$\bar{p}_N(\tau_N^-) = \left(\frac{\partial J}{\partial x_N} \right)' \quad (19)$$

Optimality conditions

$$H_i(\tau_i^-) - H_i(\tau_i^+) = 0 \quad (20)$$

$$H_N(\tau_N^-) = 0 \quad (21)$$

Conditions (20) and (21) can be used to solve for the optimal switching sequence τ_i , $i = 1, 2, \dots, N$ or the vector $[\tau_1, \dots, \tau_N]^T$. In Ref. [26], similar optimality conditions are derived for similar hybrid systems. However, here, we relax the assumption of fixed final time τ_N , which gives the additional condition (21).

4.3 Computation Algorithm. Based on the above necessary conditions for optimality, the following steepest descent algorithm can be applied to solve for the optimal layering time vector $[\tau_1, \dots, \tau_N]^T$:

- Chose initial iterate τ_i^0 for $i = 1, \dots, N$ to initialize time vector $[\tau_1, \dots, \tau_N]^T$, and chose a termination tolerance ε .
- Set iteration counter $k = 0$.
- While $|J^k - J^{k-1}| > \varepsilon$
 - (1) Compute the state trajectory $x_i(t)$, $t \in [\tau_{i-1}, \tau_i]$ for $i = 1, \dots, N$ forward in time from $t_0 = 0$ to $t_f = \tau_N$ using (10), (11), and cost J^k using (14).
 - (2) Compute the adjoining variable $\bar{p}_i(t)$, for $i = 1, \dots, N$ backward in time from $t_f = \tau_N$ to $t_0 = 0$ using (16)–(19).
 - (3) Update the time vector τ_i as follows:

$$\tau_i^{k+1} = \tau_i^k - \delta_i^k B_i, \quad \text{and}$$

$$\tau_N^{k+1} = \tau_N^k - \delta_N^k C$$

- for $i = 1, \dots, N - 1$, where δ_i^k and δ_N^k step size parameters, and $B_i = H_i(\tau_i^-) - H_i(\tau_i^+)$ and $C = H_N(\tau_N^-)$

(4)

$$k = k + 1$$

- End while
- Record the optimal layering time vector $[\tau_1, \dots, \tau_N]^T$

The optimal interlayer time (hold time between adding layers) can be computed by taking the differences between successive elements of this vector.

5 Results and Discussions

In this section, we present simulation results to demonstrate the comparative advantage of the proposed SCC approach and of its optimal layering control for UV curing of resins in a composite laminate fabrication application (fiberglass with unsaturated polyester resin). For simulations study, the associated thermal, chemical, and material constants for UV-curing of unsaturated polyester resin are extracted from published work [17,29]. For the fiberglass, E-glass thermal properties such as thermal conductivity ($k_f = 0.012 \text{ W/cm} \cdot \text{°C}$), specific heat ($c_{pf} = 0.8 \text{ J/g} \cdot \text{°C}$), and density ($\rho_f = 2.55 \text{ g/cm}^3$) are used. Volume fractions of 40% and 60% are used for fiber and resin, respectively to determine the average thermal properties of the composite laminate. The associated parameters used in simulations are summarized in Table 1.

The simulation considers the UV curing model (8) to generate the temperature and cure state distributions in all layers. A constant UV-intensity of 65 mW/cm^2 is used for the entire curing duration. For the simulation and the implementation of the optimization algorithm described above, a ten-node spatial discretization is used for each layer to convert the PDE for the temperature state to a set of ODEs. For most of the analysis, except where indicated, a total of 10 layers with a thickness of 1 mm each are considered.

First, we illustrate the advantage of the proposed SCC approach over one-shot concurrent curing (all ten layers deposited and cured at the same time). The comparison results are given in Fig. 6, which shows the final cure level distribution achieved for the ten-layer part. Two SCC versions are included: the first (case1) with the optimized layering time control (optimized inter-layer time) and the second (case 2) with equal time-interval holds between layer additions. Both have the same final time as case 1 (901 s). A desired final cure level of 90% is defined as the target for the optimized layering time controlled SCC. For the one-shot curing with overcure (case 3), the UV radiation input and the length of overall curing time is kept the same as that of the SCC. For the one-shot curing without over cure (case 4), the UV radiation input is kept the same as that of the SCC, but curing is simulated only until the top layers' cure level reaches the target level of about 90%.

As shown in Fig. 6, for both cases of one-shot concurrent curing, unacceptable cure deviation is observed between the top and

Table 1 Parameter values used in the simulations

Parameter	Variable	Value
Density of composite	ρ	1.69 g/cm^3
Specific heat of composite	c_p	$1.14 \text{ J/g} \cdot \text{°C}$
Thermal conductivity of composite	k	$0.0035 \text{ W/cm} \cdot \text{°C}$
Density of resin	ρ_r	1.1 g/cm^3
Specific heat of resin	c_{pr}	$1.674 \text{ J/g} \cdot \text{°C}$
Thermal conductivity of resin	k_r	$0.0017 \text{ W/cm} \cdot \text{°C}$
Convective heat transfer	h	$0.002 \text{ W/cm}^2 \cdot \text{°C}$
Volumetric fraction of resin	v_r	0.6
Polymerization enthalpy of resin	ΔH_r	335 J/g
Photoinitiator concentration	s	0.05%wt
UV attenuation constant	λ_c	2 (cm)^{-1}
Activation energy	E	12.7 KJ/mol
Gas constant	R	$8.314 \text{ J/mol} \cdot \text{K}$
Pre-exponential factor of rate constant	ϕ	0.631 (s)^{-1}
Ambient temperature	T_∞	25 °C
Reaction orders	m and n	0.7 and 1.3
Constants exponents	p and q	0.8 and 0.7
Absorptivity UV radiation at surface	ϑ	0.85

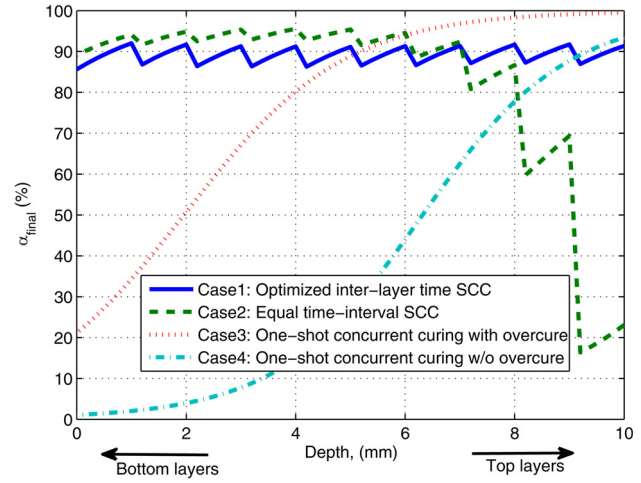


Fig. 6 Achieved final cure level profile with SCC and one-shot curing

bottom layers of this thick part. Even with over cure in the top layers, only a small cure level change happens in the bottom layers with one-shot curing. On the other hand, with SCC, the cure level deviation is significantly reduced in most layers even with equal time-interval layer addition. However, the cure level deviation in the last 2–3 top layers is unacceptable with equal time-interval layer addition, since not enough time is allocated to cure the fresh layers at the top. The designed model-based optimization algorithm compensates this effect by returning the optimal interlayer time holds that guarantee a near through cure (overall final cure deviation less than 6%) in all layers at the final time.

To study the distribution of the optimal interlayer hold times, the proposed optimization algorithm is used to generate simulation results for three cases of the same 10 mm thick part: 5, 10, and 20 layers. The results are plotted in Fig. 7. The optimal inter-layer hold time takes the same trend in all three cases. It first decreases as one adds layers from the bottom then increases for the last few top layers. The high hold time at the first bottom layer can be explained by the need to anticipate and counteract the attenuation of UV radiation in the bottom layers as new layers are add on. The highest hold time for the last top layer is explained by the need of bringing the cure level there from zero to the desired level quickly (see also Fig. 8) while the cure level continues to build in the lower layers with attenuated UV radiation.

The need for the highest interlayer hold time for the last/top layer is consistent with a related result in Ref. [15] who treated laminator temperature profile optimization for equal-time-interval layer addition for a thermal curing process and found that the highest input is needed for the top layer.

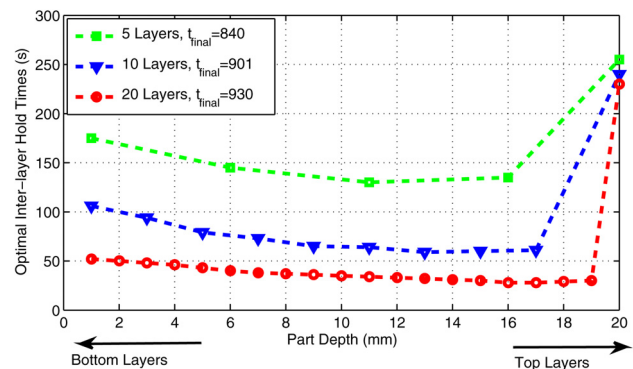


Fig. 7 Optimal interlayer hold times for three cases

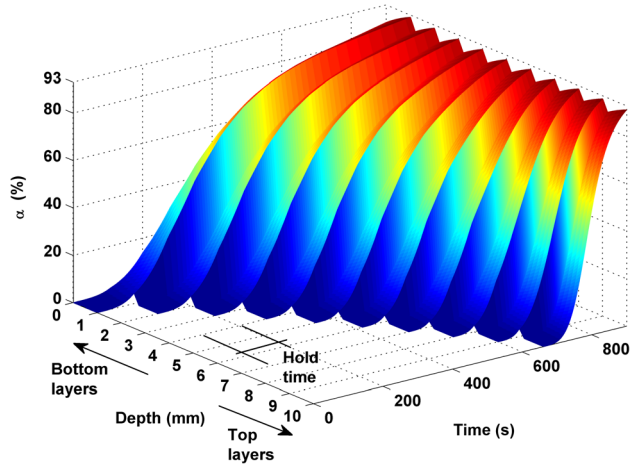


Fig. 8 Cure level profile with optimized SCC

Figure 7 also shows that while the optimal interlayer hold times are longer when using thicker layers to build the same 10 mm part, the final curing time increases slightly as the number of layers increases, with thinner layers (see t_{final} values in the legend of Fig. 7). When using thick layers, the large attenuation effect in the thick layers dominates the cure rate and therefore the interlayer hold times. When using thin layers, there is a dominant interlayer cooling effect (see Fig. 10) between a fresh layer and a previous layer, which likely contributes to the slightly longer overall cure time (sum of interlayer hold times).

The detailed space-time evolutions of the cure state and the corresponding temperature state are plotted for the optimized SCC with ten-layers for the entire curing duration of 901 s in Figs. 8 and 9, respectively. As shown in Fig. 8, after the cure initiates in the bottom layers, it continues to propagate, with albeit the attenuated UV radiation reaching the bottom, while the cure in the top layers quickly builds from zero with the direct UV radiation exposure at the top. With the optimized SCC, the optimal hold time between the layers is determined by explicitly considering the curing process dynamics in all layers so that the cure in all layers converges to close to the desired cure level in the (also optimized) final curing time.

The temperature profile, in Fig. 9, depicts the nature of the changing temperature conditions of layering in the SCC process. The addition of a new layer at ambient condition after the temperature on the previous layer is elevated to some level will lower the temperature in the layers (at least, near the interfacial nodes) because of heat transfer between layers. For ten-layer part considered here, the simulated highest possible temperature in the curing

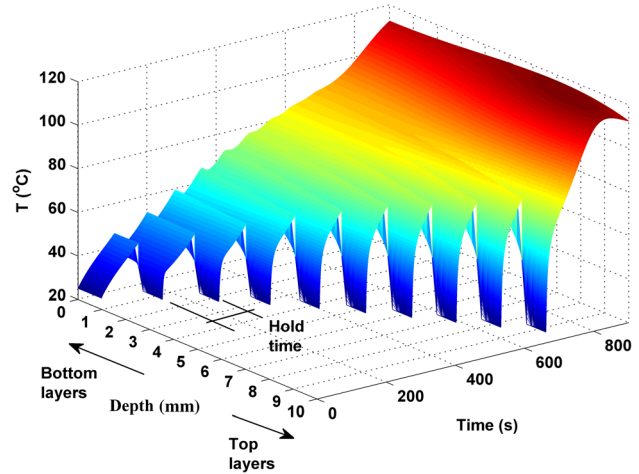


Fig. 9 Temperature profile with optimized SCC

process is less than only 120 °C which is less than the acceptable maximum fiberglass composite curing temperature (130 °C, 140 °C) targeted in the works [25,30].

To show the cooling effect due to heat transfer between layers, the evolution of temperature at selected interfaces is plotted in Fig. 10. Interface-1 represents the node between the bottom-end layer and the layer immediately on top of it and Interface-2 to Interface-9 are defined similarly as more layers are added. Two observations can be made from this result: (1) At each layer addition, the temperature of previous interfaces (and layers) reduces before it builds up again. This helps keep the overall temperatures lower. (2) For layer additions that come later in the SCC process, the temperatures in the new layers (interfaces) build rather rapidly to catch up with temperature in the previous layers and eventually exceed it, still with interlayer gradients reduced to lower than about 20 °C. This latter observation can be explained by considering the nature of UV attenuation in the multilayer part and the poor thermal conductivity of polymeric material. As new layers are added on, UV attenuation levels increase in the bottom layers. As a result, given the poor thermal conductivity, the temperature in the top layer builds faster than in the bottom layers which are exposed to attenuated UV radiation in the presence of the top layers. The rapid rise in the temperature of the top layers may indeed be objectionable and therefore needs further experimental investigation.

Finally, Fig. 11 shows the progress of the cost function to illustrate the convergence of the proposed computational algorithm. For the ten-layer part, the optimal solution is achieved to a predefined iteration tolerance value of $\epsilon = 1 \times 10^{-6}$ after 50 iterations.

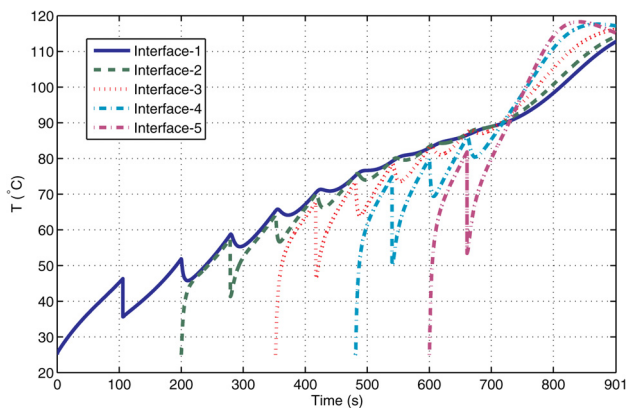


Fig. 10 Temperature evolution at selected interfaces

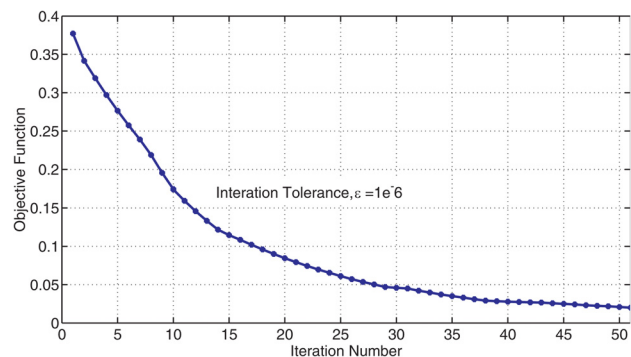


Fig. 11 Convergence of computational algorithm: Optimal cost for ten layers

6 Conclusions

This paper outlined (1) a SCC approach for layer-by-layer manufacturing of thick parts using UV radiation, (2) a systematic optimization scheme for the interlayer hold times based on a hybrid system realization of the SCC process. The motivations for SCC and that it can be optimized were outlined first. Then, the hybrid framework for deriving the optimality condition and a computational algorithm for obtaining the solution were detailed. The hybrid optimization approach was then applied to solve for the optimal interlayer hold times to achieve minimal cure level deviations across a multilayer part.

Simulation results on a composite processing application illustrated the advantages of the proposed and optimized SCC over simple layering one-shot curing as well as an equal time-interval SCC in achieving the target cure level with minimal deviation across all layers. It is also shown that the optimal interlayer hold times are not all the same but do show a pattern of being lower for middle layers and being longer for the bottom most and top most layers. Other observations are also made regarding interlayer cooling with the SCC approach that helps to reduce overall temperatures and to quickly remove thermal gradients in the multilayer part.

Finally, the authors remark on possible extensions of the approach proposed in the paper. The presented work dealt with off-line model-based optimization. However, varying model parameters such as reaction orders and activation energy may affect the accuracy of this off-line optimization results. To overcome this, the authors are pursuing a modification of the algorithm by including explicit parametric sensitivity considerations for a result that is robust to parameter variations from the outset. Another extension being pursued by the authors is the coupled optimization of the UV radiation input for each layer along with the interlayer hold times.

Acknowledgment

This research has been supported, in part, by the National Science Foundation under Grant No. CMMI-1055254 and the U.S. Department of Energy's GATE Program under Grant No. DE-EE0005571.

Appendix

Generally, for two or more layers, interface conditions are required to capture the heat transfer between layers. These interface conditions are

$$\left[k_z \frac{\partial T(j = \bar{n}_i/2)}{\partial z} \right]_{\text{new layer}} = \left[k_z \frac{\partial T(j = \bar{n}_i/2)}{\partial z} \right]_{\text{pervious layer}}, \quad i = 1, \dots, N - 1 \quad (\text{A1})$$

and, at the interface nodes, the temperatures are constrained to be equal

$$[T(j = \bar{n}_i/2)]_{\text{new layer}} = [T(j = \bar{n}_i/2)]_{\text{pervious layer}}, \quad i = 1, \dots, N - 1 \quad (\text{A2})$$

The PDE–ODE system in Eq. (8) can be converted to set of ODES using central difference approximations for the spatial derivative in the PDE. For two or more layers, the major changes to Eq. (8) are that the bottom BC of the new layer and the top BC of the pervious layer are substituted for by interface conditions (A1) and (A2). Assuming constant thermal properties such as k_z , ρ , and c_p , we can write an explicit form of f_i for i -layers (i th-mode) as given below

$$f_i^T = \begin{bmatrix} -(c_T + 2)a & 2a & 0 & 0 & \dots & 0 \\ a & -2a & a & 0 & \dots & 0 \\ 0 & a & -2a & a & \dots & 0 \\ \vdots & \vdots & \vdots & \vdots & \vdots & \vdots \\ 0 & \dots & 0 & a & -2a & a \\ 0 & \dots & 0 & 0 & 2a & -2a \end{bmatrix} \begin{bmatrix} T_1 \\ T_2 \\ \vdots \\ T_j \\ \vdots \\ T_{\bar{n}_i/2} \end{bmatrix} + b \begin{bmatrix} \dot{\alpha}_1 \\ \dot{\alpha}_2 \\ \vdots \\ \dot{\alpha}_j \\ \vdots \\ \dot{\alpha}_{\bar{n}_i/2} \end{bmatrix} + a \begin{bmatrix} c_T T_\infty + c_1 I_0 \\ 0 \\ 0 \\ \vdots \\ 0 \\ 0 \end{bmatrix} \quad (\text{A3})$$

$$f_i^z = d \begin{bmatrix} \exp(-E/R(T_1 + 273))\alpha_1^m (1 - \alpha_1)^n \exp(-\lambda_c * 0) I_0^p \\ \exp(-E/R(T_2 + 273))\alpha_2^m (1 - \alpha_2)^n \exp(-\lambda_c * dz) I_0^p \\ \vdots \\ \exp(-E/R(T_j + 273))\alpha_j^m (1 - \alpha_j)^n \exp(-\lambda_c * (j - 1)dz) I_0^p \\ \vdots \\ \exp(-E/R(T_{\bar{n}_i/2} + 273))\alpha_{\bar{n}_i/2}^m (1 - \alpha_{\bar{n}_i/2})^n \exp(-\lambda_c * (\bar{n}_i/2 - 1)dz) I_0^p \end{bmatrix} \quad (\text{A4})$$

where $a = k_z/dz^2 \rho c_p$, $b = v_r \Delta H_r \rho_r / \rho c_p$, $c_T = 2dz h / k_z$, $c_1 = 2dz \theta / k_z$, $dz = l / (\bar{n}_i/2 - 1)$, $d = \phi s^q$. Note that, $\bar{n}_i/2$ is an integer since \bar{n}_i defines the dimension of state x that augment both temperature and cure level at each spatial node.

The form of the state matrix in f_i^T given in Eq. (A3) is a tri-diagonal symmetric matrix when the thermal properties are assumed constant across layers. The matrix loses symmetry for varying thermal properties and the interface nodes

in f_i^T need to be updated accordingly. The derivation for this case simply follows the above discussion and is omitted here.

References

- [1] Perry, M. F., and Young, G. W., 2005, "A Mathematical Model for Photopolymerization From a Stationary Laser Light Source," *Macromol. Theory Simul.*, **14**(1), pp. 26–39.

- [2] Roose, P., Fallais, I., Vandermiers, C., Olivier, M.-G., and Poelman, M., 2009, "Radiation Curing Technology: An Attractive Technology for Metal Coating," *Prog. Org. Coat.*, **64**(2–3), pp. 163–170.
- [3] Compston, P., Schiemer, J., and Cvetanovska, A., 2008, "Mechanical Properties and Styrene Emission Levels of a UV-Cured Glass-Fibre/Vinylester Composite," *Compos. Struct.*, **86**(1), pp. 22–26.
- [4] Endruweit, A., Johnson, M. S., and Long, A. C., 2006, "Curing of Composite Components by Ultraviolet Radiation: A Review," *Polym. Compos.*, **27**(2), pp. 119–128.
- [5] Cunico, M. W. M., and de Carvalho, J., 2013, "Optimization of Thick Layers Photopolymerization Systems Applying Experimental and Analytical Approach," *Rapid Prototyping J.*, **19**(5), pp. 337–343.
- [6] Wenbin, H., Tsui, L. Y., and Haiqing, G., 2005, "A Study of the Staircase Effect Induced by Material Shrinkage in Rapid Prototyping," *Rapid Prototyping J.*, **11**(2), pp. 82–89.
- [7] Duan, Y., Li, J., Zhong, W., Maguire, R. G., Zhao, G., Xie, H., Li, D., and Lu, B., 2012, "Effects of Compaction and UV Exposure on Performance of Acrylate/Glass-Fiber Composites Cured Layer by Layer," *J. Appl. Polym. Sci.*, **123**(6), pp. 3799–3805.
- [8] Campanelli, S. L., Cardano, G., Giannoccaro, R., Ludovico, A. D., and Bohez, E. L. J., 2007, "Statistical Analysis of the Stereolithographic Process to Improve the Accuracy," *Comput.-Aided Des.*, **39**(1), pp. 80–86.
- [9] Endruweit, A., Ruijter, W., Johnson, M. S., and Long, A. C., 2008, "Transmission of Ultraviolet Light Through Reinforcement Fabrics and Its Effect on Ultraviolet Curing of Composite Laminates," *Polym. Compos.*, **29**(7), pp. 818–829.
- [10] Paul, R., Anand, S., and Gerner, F., 2014, "Effect of Thermal Deformation on Part Errors in Metal Powder Based Additive Manufacturing Processes," *ASME J. Manuf. Sci. Eng.*, **136**(3), p. 031009.
- [11] Wang, X., 1999, "Calibration of Shrinkage and Beam Offset in SLS Process," *Rapid Prototyping J.*, **5**(3), pp. 129–133.
- [12] Navangul, G., Paul, R., and Anand, S., 2013, "Error Minimization in Layered Manufacturing Parts by Stereolithography File Modification Using a Vertex Translation Algorithm," *ASME J. Manuf. Sci. Eng.*, **135**(3), p. 031006.
- [13] Verriest, E. I., 2012, "Pseudo-Continuous Multi-Dimensional Multi-Mode Systems," *Discrete Event Dyn. Syst.*, **22**(1), pp. 27–59.
- [14] Xu, X., and Antsaklis, P. J., 2004, "Optimal Control of Switched Systems Based on Parameterization of the Switching Instants," *IEEE Trans. Autom. Control*, **49**(1), pp. 2–16.
- [15] Klosterman, D., Chartoff, R., Flach, L., and Bryant, E., 2000, "Model-Based Control of Cure Distribution in Polymer Composite Parts Made by Laminated Object Fabrication (LOF)," *Solid Freeform Fabrication Proceedings*, University of Texas at Austin, Austin, TX, pp. 409–416.
- [16] Decker, C., 2001, "UV-Radiation Curing Chemistry," *Pigm. Resin Technol.*, **30**(5), pp. 278–286.
- [17] Matias, J. M., Bartolo, P. J., and Pontes, A. V., 2009, "Modeling and Simulation of Photofabrication Processes Using Unsaturated Polyester Resins," *J. Appl. Polym. Sci.*, **114**(6), pp. 3673–3685.
- [18] Tang, Y., 2005, "Stereolithography Cure Process Modeling," Ph. D. dissertation, Georgia Institute of Technology, Atlanta, GA.
- [19] Hong, W., Lee, Y. T., and Gong, H., 2004, "Thermal Analysis of Layer Formation in a Stepless Rapid Prototyping Process," *Appl. Therm. Eng.*, **24**(2), pp. 255–268.
- [20] Wang, X., 2001, "Modeling of In-Situ Laser Curing of Thermoset-Matrix Composites in Filament Winding," Ph. D. dissertation, University of Nebraska, Lincoln, NE.
- [21] Bowman, M. D. G. C. N., 2002, "Development of a Comprehensive Free Radical Photopolymerization Model Incorporating Heat and Mass Transfer Effects in Thick Films," *Chem. Eng. Sci.*, **57**(5), pp. 887–900.
- [22] Schwalm, R., 2006, *UV Coatings: Basics, Recent Developments and New Applications*, Elsevier, Amsterdam.
- [23] Yebi, A., and Ayalew, B., 2014, "Process Control for UV Curing of Thick Film Resins in Polymer Composite Laminates," *ASME J. Dyn. Syst. Meas. Contr.* (to be published).
- [24] Miller, G. A., Gou, L., Narayanan, V., and Scranton, A. B., 2002, "Modeling of Photobleaching for the Photoinitiation of Thick Polymerization Systems," *J. Polym. Sci., Part A: Polym. Chem.*, **40**(6), pp. 793–808.
- [25] Parthasarathy, S., Mantell, S. C., and Stelson, K. A., 2004, "Estimation, Control and Optimization of Curing in Thick-Sectioned Composite Parts," *ASME J. Dyn. Syst. Meas. Contr.*, **126**(4), pp. 824–833.
- [26] Mehta, T. R., Yeung, D., Verriest, E. I., and Egerstedt, M., 2007, "Optimal Control of Multi-Dimensional, Hybrid Ice-Skater Model," *American Control Conference*, IEEE, pp. 2787–2792.
- [27] Liu, J., Zhang, K., Sun, C., and Wei, H., 2013, "Second Order Transition-Time Optimization for Switched Dynamical Systems," *32nd Chinese Control Conference*, IEEE, pp. 2382–2386.
- [28] Kirk, D. E., 2004, *Optimal Control Theory: An Introduction*, Dover Publications, Mineola, NY.
- [29] Bártolo, P., 2001, "Optical Approaches to Macroscopic and Microscopic Engineering," Ph.D. dissertation, University of Reading, Reading, UK.
- [30] Dufour, P., Michaud, D. J., Touré, Y., and Dhurjati, P. S., 2004, "A Partial Differential Equation Model Predictive Control Strategy: Application to Autoclave Composite Processing," *Comput. Chem. Eng.*, **28**(4), pp. 545–556.